HHS Public Access

Author manuscript

Anal Bioanal Chem. Author manuscript; available in PMC 2016 August 23.

Published in final edited form as:

Anal Bioanal Chem. 2015 November ; 407(27): 8291–8301. doi:10.1007/s00216-015-8800-5.

Combined fiber probe for fluorescence lifetime and Raman spectroscopy

Sebastian Dochow[1], **Dinglong Ma**[2], **Ines Latka**[1], **Thomas Bocklitz**[1], **Brad Hartl**[2], **Julien Bec**[2], **Hussain Fatakdawala**[2], **Eric Marple**[4], **Kirk Urmey**[4], **Sebastian Wachsmann-Hogiu**[3], **Michael Schmitt**[1], **Laura Marcu**[2], and **Jürgen Popp**[1,5]

[1] Institute of Physical Chemistry and Abbe Center of Photonics, Friedrich Schiller University Jena, Helmholtzweg 4, 07743 Jena, Germany

[2] Department of Biomedical Engineering, University of California, Davis, 451 E. Health Sciences Drive, Davis, CA 95616, USA

[3] Department of Pathology and Laboratory Medicine and Center for Biophotonics, University of California, Davis, 2700 Stockton Blvd., Sacramento, CA 95817, USA

[4] EmVision LCC, 1471 F Road, Loxahatchee, FL 33470, USA

[5] Leibniz Institute of Photonic Technology Jena e.V., Albert-Einstein-Str. 9, 07745 Jena, Germany

Abstract

In this contribution we present a dual modality fiber optic probe combining fluorescence lifetime imaging (FLIm) and Raman spectroscopy for in vivo endoscopic applications. The presented multi-spectroscopy probe enables efficient excitation and collection of fluorescence lifetime signals for FLIm in the UV/visible wavelength region, as well as of Raman spectra in the near-IR for simultaneous Raman/FLIm imaging. The probe was characterized in terms of its lateral resolution and distance dependency of the Raman and FLIm signals. In addition, the feasibility of the probe for in vivo FLIm and Raman spectral characterization of tissue was demonstrated.

Keywords

Fluorescence lifetime; Raman spectroscopy; Bimodal; Imaging; Fiber probes

Introduction

Ideally, endoscopists should be able to detect and characterize suspicious tissue regions during the operation procedure and take biopsies and resections only where necessary. However, under conventional endoscopic white-light inspection premalignant conditions and

Laura Marcu lmarcu@ucdavis.edu, Jürgen Popp juergen.popp@uni-jena.de.

Electronic supplementary material The online version of this article (doi:10.1007/s00216-015-8800-5) contains supplementary material, which is available to authorized users.

Compliance with ethical standards All procedures performed in studies involving animals were in accordance with the ethical standards of the institution or practice at which the studies were conducted. The Illinois Institutional Animal Care and Use Committee (IACUC) guidelines of all University of California institutions were followed.

early forms of cancer are difficult to detect and are frequently overlooked [1]. In order to overcome this drawback molecular spectroscopy can be utilized to generate molecular/chemical images. In this context, fluorescence and Raman spectroscopy have been established for modern biomedical imaging, as they provide morphological information based on molecular contrast [2, 3].

Within the last 10 years Raman spectroscopy has been recognized as a valuable biomedical analytical tool for spectroscopic diagnostics of diseases and for studying biological tissue in general [3–5]. Because every chemical species in a tissue sample has a unique Raman spectrum, the overall chemical composition of the tissue sample can in principle be evaluated through an analysis of the Raman spectra of the sample by using sophisticated chemometric data analysis [6]. Nowadays Raman microscopy has been used on biopsy samples of virtually every organ and its great capability for objective evaluation of tissue samples for early diagnosis of disease, particularly cancer, has been demonstrated [3]. The potential to couple a Raman spectrometer to optical fibers for single point measurements adds a unique potential to the detection technique, and enables remote sensing along with flexibility of sample or probe positioning [7]. In many medical applications the accessibility of a particular tissue spot and the size of the intra-surgical probe are restricted, because of the anatomy of the site of interest, as for instance during colonoscopy or cardiovascular endoscopy. The use of optical fibers makes the positioning and the collection of the spectral information much easier and more convenient compared to free-beam optics. Real-time in vivo applications of Raman fiber probes for clinical diagnosis of different types of cancers, including skin, lung, stomach, esophageal, colorectal, cervical, and breast cancers, were recently summarized by Wang et al. [8]. The most challenging drawback of spontaneous Raman spectroscopy is the weak Raman signal intensity, which leads to rather long measurement times of a few seconds per measurement point. One approach to address this issue for in vivo applications is to combine Raman spectroscopy with imaging methodologies able to provide an initial faster assessment of tissue biochemical or morphological features, as for instance optical coherence tomography (OCT) [9], fluorescence spectroscopy [10], fluorescence lifetime imaging (FLIm), ultrasound or diffuse reflectance spectroscopy [11]. The fast imaging methodology can provide an overview image to identify suspicious tissue areas (“red flags”) that subsequently can be analyzed in detail by Raman spectroscopy. Several research groups have been working on the development of such multimodal “red flag” endoscopic Raman probes, such as OCT combined with Raman [9], intrinsic fluorescence and/or diffuse reflectance spectroscopy and Raman [12, 13].

FLIm is one optical imaging modality which can easily be implemented in fiber optic probes [14, 15]. FLIm provides information on the chemical composition of tissue based on the emission (spectra intensities and lifetimes) of certain endogenous fluorophors such as nicotinamide adenine dinucleotide (NADH), flavin adenine dinucleotide (FAD), collagen, elastin, and others [16]. Recent implementations of FLIm allow a rapid data acquisition [17]. One major advantage of FLIm is that the fluorescence lifetime is not affected by changes in fluorescence intensity. Therefore, FLIm measurements are minimally affected by changes in probe to target distance [18]. FLIm is predestinated for combination with Raman spectroscopy into a single fiber optical probe for the rapid and simultaneous interrogation of

large tissue areas with molecular specificity in single points or clusters of a presegmented image.

In this study we report, to the best of our knowledge, for the first time a fiber optical probe combining Raman spectroscopy with fluorescence lifetime spectroscopy for a FLIm-guided acquisition of Raman spectra. In the following sections we describe the probe design along with the associated lateral resolution and distance dependencies of the signals measured using the described probe design. The validation of the FLIm/Raman probe on various animal tissue samples and its capability to discriminate between different tissue types (i.e., bone, fat, and muscles) are presented. Finally, in vivo Raman spectra obtained with FLIm guidance from the brain of a rat as well as surrounding tissues are demonstrated.

Material and methods

FLIm/Raman probe design

The multi-spectroscopy FLIm/Raman probe (EmVision, Loxahachee, FL) is similar in design to the probe described in detail in US patents 8,175,423 and 8,702,321. Figure 1a and b show illustrations of the probe design utilizing a focusing lens, allowing for the measurement areas of the two different spectroscopic modalities to be obtained from the same spot. The probe consists of two 300-μm-core fibers (green) for FLIm, as well as one excitation (red) and seven collection (blue) 300-μm-core fibers for Raman spectroscopy. A donut-shaped long-pass filter is positioned in front of the seven Raman collection fibers to reject the laser light. The Raman laser delivery fiber has a small band-pass filter positioned in front of it. The fibers, lens, and other components are placed inside a stainless steel 14-gauge extra-thin-wall needle tube (0.072 in. ID, 0.083 in. OD).

Instrumental setup

The overall FLIm/Raman setup is schematically sketched in Fig. 1c showing the FLIm setup and the three-channel wavelength selection module (upper part) and the Raman probe setup (lower part). The probe itself was mounted to an xyz stage (Thorlabs, USA) which allows positioning of the probe on single spots and a controlled motion over the sample area. The FLIm acquisition time was matched to the time frame of the Raman spectrometer rate, by adapting the amount of mean FLIm spectra per point to reach the same amount of spectra per line for both modalities. The speed of FLIm had to be decreased by more than two orders of magnitude to match the frame rate necessary for the detection of the Raman scattering. The total repetition rate for both modalities was determined to be 40 Hz and was limited by the acquisition and readout time of the Raman spectrometer. All subsequent images were taken as raster scans utilizing the x- and y-axes of the stage. These maps consist of separately triggered line scans with a matched amount of pixels per line. Both modalities were acquired simultaneously for all shown images.

Fluorescence is generated via excitation with a fiber laser (Fianium HE, 355 nm, 80 ps, 10 kHz–1 MHz, 0.5 μJ). The fluorescence emission is spectrally resolved using a custom-made wavelength selection module (WSM) [16] that separates the fluorescence into four wavelength channels (center wavelength/bandwidth 390/40, 452/45, 542/50, and 629/53 nm)

coupled to four optical delay lines (lengths 1, 10, 19, and 28 m), generating a 45-ns delay between each channel. The fluorescence photons from all four channels were detected using a single micro-channel plate (MCP) photomultiplier (PMT) (R3809U-50, Hamamatsu, 45 ps FWHM). The resulting signal output is then amplified (pre-amplifier C5594, Hamamatsu, 36 dB) and digitized (digitizer PXIe-5185, National Instrument, 12.5 GS/s sampling rate, 3 GHz analog bandwidth). An embedded controller (PXIe-8102, National Instrument) was integrated with the digitizer for readout, processing, and storage of the multi-spectral time-resolved fluorescence spectroscopy (ms-TRFS) data. The excitation pulse power was set to 200 μJ and kept constant throughout the experiments.

The Raman probe excitation fiber was coupled to a 300-mW multi-mode laser (B&W Tec) with a coupling efficiency of 70 %. The overall Raman excitation power was set to 100 mW at the sample and also kept constant during all acquisitions except for the in vivo measurements for which the power was set to 50 mW to prevent sample drying. The collection fiber port was connected to a compact Raman spectrometer RXN1 (Kaiser Optical Systems) equipped with a 785-nm transmission grating (LGP785, Kaiser Optical Systems) and a Pixis400B CCD (Princeton Instruments). The CCD was thermoelectrically cooled to −70 °C. The readout signal was collected with full vertical binning. All acquisitions were triggered by the FLIm software, which was modified to send a line starting trigger to the CCD camera and each data set was recorded by the visual basic scripting of the Winspec software and automatically saved.

FLIm/Raman data evaluation

The images presented were recorded as raster scans with different lateral step sizes. Each step generates a pixel. For each pixel in the FLIm image and the fluorescence decays were recovered by deconvolution of the instrument impulse response function (iIRF) from the measured fluorescence pulse transients. The iIRF characterizes the overall broadening of the fluorescence pulse due to optical dispersion and electronics [18]. For deconvolution we employed a fast algorithm (<1 ms per decay) previously reported by our group [19]. The algorithm is based on a constrained least-squares deconvolution with a Laguerre expansion (CLSD-LE) method and has demonstrated its robustness against noise. To combine the fluorescence intensity and lifetime information of the FLIm images, intensity weighting on lifetime color maps was implemented. The alpha channel of the RGB colored lifetime image was modulated on the basis of the normalized fluorescence intensity.

Since the recorded Raman spectra showed a fluorescence background as well as strong zero-order residuals from the transmission grating due to grating imperfections, an extensive Raman data pre-processing was necessary. First, a Gaussian kernel smoothing with a bandwidth of approx. 3 cm^{-1} was applied. Thereafter, a background estimation based on the statistic-sensitive, non-linear iterative peak-clipping (SNIP) algorithm was carried out. Subsequently, the spectra were truncated to the wave-number region between 462 and 1991 cm^{-1} followed by vector normalization. A principal component analysis was used to reduce the dimension to 20 scores and to eliminate the noise. A k-means cluster analysis with k=10 was performed and the results were then plotted in false color maps.

Probe validation

Probe characterization—In order to determine the minimal resolvable sample area of the probe, the lateral resolution of both modalities needs to be determined. The lateral resolution was measured by mapping a Starfrost slide (Light Lab, USA) as a sample, as it contains several edges of different chemical composition which at the same time show different fluorescence lifetimes. In order to determine the resolution of the probe, the structures were oversampled by a 42.5-μm raster scan in the x and y-axes. The acquisition time per Raman spectra was set to 20 ms. The FLIm acquisition time was matched to the same frame rate by adapting the mean number of FLIm spectra per point to reach the same number of points (spectra) per line for both modalities. Both signals were acquired at the same time.

FLIm/Raman bimodal mapping—To compare the overlap between the FLIm and Raman acquisitions, images were recorded on tissue samples with diverse compositional features, such as bone, fat, muscle, and connective tissue. For practical reasons commercially available (prepared for consumption) samples of beef and lamb meat were used. The fluorescence and Raman spectroscopic contrast in such samples are expected to be generated by collagen and elastin in connective tissues, bone, various lipid components, and lipoproteins in fat. The samples were prepared by flattening the tissue surface and by fixation on a foam adaptive holder in order to preserve the surface during the acquisition time of the bimodal raster scan. The sample was aligned to the scanning plane with a two-axis tilting stage. Several raster scans with dimensions of 50×50 mm, which corresponds to 400×400 spectra for both modalities, were acquired. The Raman acquisition time was again set to 20 ms and the FLIm speed was synchronized in order to generate the same number of FLIm and Raman readout points per line.

In vivo Raman spectra acquisition with FLIm guidance—For the in vivo experiments, all animal care and procedures were performed in accordance with the protocol that was reviewed and approved by the Institutional Animal Care and Use Committee (IACUC) of the University of California, Davis. Healthy Fischer 334 rats (Charles River Laboratories Inc., Wilmington, MA, USA) were anesthetized with isoflurane and placed in a stereotaxic frame equipped with a nose cone. A unilateral craniotomy was then performed on the animal using a high speed rotatory tool to expose the brain tissue. In order to reduce bleeding in the imaging field and maintain physiologically representative conditions, the animal's dura mater was left intact for the experiments. FLIm/Raman bimodal in vivo maps of the dura were recorded. While the Raman excitation power was decreased from 100 to 50 mWas compared to the ex vivo tissue experiments the acquisition time was kept at 20 ms per Raman spectrum. The low excitation and the short measurement time were chosen to prevent the brain from drying during the acquisition of a map, which took about 2 min in total.

Subsequently, several FLIm-guided single point Raman spectra with longer acquisition times (0.1 s and 10 acquisitions) were recorded to demonstrate the performance of the probe. The points for the Raman measurements were guided by FLIm measurements (e.g., changes in lifetime in one of the channels or changes in intensity) for different tissue areas within and around the craniotomy window of the rat. The FLIm repetition frequency was set to the typical value of 10 kHz to locate different tissue sites at the fastest possible speed. For the

single point Raman measurements, the probe was removed from the stage and guided by hand.

Results and discussion

Probe characterization

The images of a raster scan of the Starfrost sample are shown in Fig. 2a depicting the clustered Raman image in the upper part and the fluorescence intensity image below. The resolution was determined on the basis of the 10–90 % signal increase/decrease at an interface edge, by plotting a fitted erfc (error) function for the Raman image and a direct intensity profile for the fluorescence image. In each of these images 10 sample lines at different material interfaces were chosen to determine the spatial resolution. The average lateral resolution is 5.6 image pixels, which corresponds to 240 μm, for the Raman channels and 6.2 image pixels, which corresponds to 260 μm, for the FLIm channels of the probe.

The distance dependencies of both Raman and fluorescence intensities of the probe were acquired on the same sample during a pullback sequence with a step size of 10 μm. The results are shown in Fig. 2c. The Raman intensity corresponds to the integrated area of the most prominent Raman peak at 810 cm^{-1} and was plotted in blue against the distance to the sample. The same was carried out for the fluorescence intensity of channel 1 (Fig. 2c, red curve). The optimal working distance of the Raman channel was determined to be in contact with the sample in accordance with the highest collection efficiency. Since the fluorescence lifetime can be extracted even at low signal levels, the dependency of the Raman signal is the limiting factor for the probe.

For the following bimodal FLIm/Raman experiments the raster scan parameters in the x- and y-axes were matched to the determined resolution of 250 μm. To account for varying sample topography when working with tissue samples, the working distance was set to 0.5 mm for the subsequent bimodal mapping experiments in order to perform bimodal raster scans. The spectral quality of the Raman signal will suffer from a higher distance, but will still enable image comparison in between the two modalities.

FLIm/Raman bimodal mapping

Several raster scans with dimensions of 50×50 mm, which corresponds to 400×400 spectra for both modalities, were acquired. Typical results are shown in Fig. 3. Both modalities (i.e., FLIM and Raman) show excellent overlap within the resolution ranges mentioned above. For enhanced visualization of structural features the intensity-weighted lifetime maps are also plotted in Fig. 3 (bottom panels). Several scanning artifacts are visible in all maps, which are caused by the small probe to sample distance. These stripe-like artifacts in both modalities were induced by non-uniform tissue surfaces that resulted in close contact between the tissue and the distal end of the probe during the scanning operation.

Conventional pictures of the biological samples corresponding to the scanned area are shown in Fig. 3 (top row). The second row depicts the generated *k*-mean images with 10 clusters for the Raman spectra of the sample area. Current results show that distinct compositions of tissue samples (e.g., bone, fat, muscle) are associated with distinct Raman spectra. In

particular, bone and fat, which have a high Raman scattering cross section, are clearly distinguishable. The middle row panels show the fluorescence lifetime images. The FLIm measurements demonstrate that distinct tissue compositions can be resolved using the fluorescence lifetime maps and are cross-correlated with the Raman image. The images acquired in channel 1 (most sensitive to collagen fluorescence) demonstrate that bone-associated areas (rich in collagen) present lifetimes of about 6 ns, which is consistent throughout all samples. In contrast, the fat-associated areas (rich in various lipid constituents and lipoproteins) fluoresce primarily in channels (CH) 2 and 3 and present a broader range of lifetime values (5–8 ns). The intensity-weighted lifetime images confirm the low intensity contribution of muscle tissues. Overall, both the FLIm and the Raman images show a strong correlation in resolving distinct biochemical, morphological, and structural features within the tissue samples. The FLIm channels can be used to find suspicious lesions (presegmentation), whereas the Raman channels can be used to validate variations within the tissue, as this mode is more sensitive for detecting compositional changes.

In vivo Raman spectra with FLIm guidance

Figure 4 displays a FLIm/Raman bimodal in vivo map of a rat cortex with an adjacent dura; thus the spectroscopically sampled volume includes the gray matter covered by the thin layer of dura mater.

The fluorescence lifetime of the cortex (CH1, 3±0.17 ns; CH2, 2.17±0.17 ns; CH3, 2.27±0.15 ns) is rather uniform since the images there taken from a healthy rat brain. The longer lasting fluorescence lifetime in CH1 when compared with CH2 and CH3 is most likely due to the presence of collagen in the dura that contributes to the fluorescence emission in this wavelength band/channel [20]. The fluorescence emissions in CH2 and CH3 are most likely dominated by NAD(P)H and FAD fluorescence, respectively [21, 22]. The blood vessels at the cortex surface can be also observed owing to high absorption of the excitation laser light which results in artery-shaped structures that can be primarily observed in the intensity-weighted lifetime images. The side regions of the craniotomy can be also distinguished, because bone presents significantly longer lifetime values (CH1, 5.03±0.15 ns; CH2, 4.76±0.08 ns) because of its high collagen content. As the brain tends to swell after the skull bone is removed, the distance from the head bone to the highest point of the tissue is longer than the working distance for both modalities. Therefore, both modalities show a decreased intensity from the center of the craniotomy toward the edge (bone) as depicted in Fig. 4.

As a result of the reduced Raman excitation power (50 mW), the short acquisition time (20 ms), and the sample to probe distance, the Raman spectra quality of the raster scan is very poor. The signal to noise ratio (SNR) of several single spectra was calculated [23]. For the bone areas this was found to be 26.1±8.1 (954 cm^{-1}) and for the brain regions it is 11.0±2.7 (1440 cm^{-1}). Example spectra for both regions are shown in the Electronic Supplementary Material (ESM), Fig. S1. As a result of the high scattering cross section of lipids and bone the cross correlation between FLIm and Raman could be demonstrated. To acquire high-quality Raman spectra, the probe has to be in contact with the sample and the integration time has to be longer. Therefore, after the raster scanning the bimodal probe was removed

from the xyz stage and guided by hand. The FLIm setup was set to 10 kHz. Different tissue types in and around the craniotomy were determined by either changes of the lifetime values in one or more channels (cortex: CH1, 3±0.17 ns; CH2, 2.17±0.17 ns; bone: CH1, 5.03±0.15 ns; CH2, 4.76±0.08 ns) or a significant drop of the fluorescence intensity (which indicates blood or blood vessels). The probe was brought into contact with these sample points and the integration time was increased (0.1 s and 10 acquisitions). The FLIm-guided Raman spectra are shown in Fig. 5: Raman spectra recorded from the skull (a) brain cortex with intact dura, as well as from the visible blood vessel in the cortex (b) and several spectra from the surrounding skin (c). The spectral Raman features clearly separate all tissue types from each other and are in good agreement with previously reported results [24–27].

The two blue spectra in Fig. 5a show typical bone spectra. The Raman peaks at 585, 954, and 1050 cm^{-1} can be assigned to PO_4^{3-}, while the band around 1240–1340 cm^{-1} is due to the amide III band. The amide I band between 1655 and 1690 cm^{-1} is also clearly visible [24]. The Raman spectra presented in Fig. 5b were measured at two different locations and are related to grey brain matter (green) [25] and blood contributions from the vessel (red) which was present at the surface of the brain tissue. Blood shows resonance Raman contributions. At an excitation wavelength of 785 nm, this is an often observed phenomenon. However, the spectral resolution of the Raman setup (about 10 cm^{-1} per pixel) is not ideal for monitoring these typical narrow resonance peaks. Therefore these resonance-enhanced Raman peaks appear as much wider bands (Fig. 5b, red spectra). The spectral contributions from blood of the vessel on the surface of healthy brain tissue (red) can be assigned to the bands 685, 750 as well as 1224 and 1350 cm^{-1}. The most obvious changes can be seen at 1550–1660 cm^{-1}. All changes are in good agreement with the Raman spectra of deoxygenated blood cells [26]. Typical healthy skin spectra are shown in Fig. 5c. All contributions as for instance the amide I and amide III, as well as other contributions in the fingerprint region, e.g., the phenylalanine band at 1003 cm^{-1} which is visible in all spectra, are comparable to formerly reported results [27].

Conclusion

The combination of Raman spectroscopy with FLIm within a single fiber optical bundle probe for the simultaneous acquisition of both signals was successfully demonstrated. The achievable lateral resolution of both components (Raman and FLIm) of the probe is about 250 μm. The exact value for the resolution averaged over 10 points is 240 μm for the Raman modality and 260 μm for the fluorescence channel. Both modalities show exponential intensity decay to 20 % over a distance of 1.3 mm to the sample. Measurements conducted in tissue samples demonstrated a good correlation and spatial overlap between the FLIm and Raman spectroscopic images. Similar results were obtained for in vivo measurements of a rat brain. Finally, FLIm-guided Raman spectra were acquired and show the capabilities of FLIm-guided Raman spectral acquisition following a craniotomy procedure. This experiment demonstrated that FLIm can enable fast detection of different tissue types. Thus targeted Raman spectra can be recorded. This experiment mimics situations encountered during surgical procedures.

In the current design the FLIm excitation is emitted with a divergence angle of about 15°. This leads to lower fluorescence intensities and lower lateral resolution at higher probe to sample distances as a result of the divergence of the excitation beam. An emission under an angle of about 10° to the optical axis of the probe is not ideal, since higher probe to sample distances (>1 mm) will lead to a direction mismatch between the Raman and FLIm signals. For signal optimization both modalities require a central probe emission with nearly collimated beams and both modalities should be optimized with respect to their specific advantages. A probe with collimated FLIm excitation would allow working distances greater than 3 mm which would improve the handling for the presegmentation. Subsequently the probe will be brought into contact with the tissue in order to obtain high-quality Raman spectra.

In summary, the current study demonstrates a bimodal system for label-free spectroscopic imaging of biological tissues. An important advantage of the system is that it provides rapid characterization of a tissue's biochemical features (via FLIm) that can be used to guide a technique with high chemical specificity but slow data acquisition speed for improved characterization/diagnosis of specific areas of interest. This approach addresses the need for techniques that, for example, can rapidly detect suspicious areas/lesions to generate a spectroscopic image of the lesion and the surrounding tissue. The extent of such lesions (field cancerization or early malignant transformations) can then be assessed by Raman spectroscopy that can provide a more specific characterization than FLIm. In this combination FLIm and Raman spectroscopy can complement each other in providing a fast and highly specific biomedical imaging technique.

Supplementary Material

Refer to Web version on PubMed Central for supplementary material.

Acknowledgments

Current study was supported in part by National Institute of Health grants R21 CA178578 and R01 CA187427. Financial support of the Bundesministerium für Bildung und Forschung for the project “Fiber Health Probe” is highly acknowledged (FKZ: 13N1225, 3N12526), as well as the financial sponsorship of the Carl-Zeiss-Stiftung.

Biography

Sebastian Dochow studied physical technologies and laser and optotechnologies at Ernst Abbe University of Applied Sciences and graduated in both. After his master thesis he worked for several years in the field of gas discharge plasma technologies in particular metrology and imaging of extreme ultraviolet sources. In 2009 he joined the Leibniz

Institute of Photonic Technology in the Department of Spectroscopy and Imaging working on microfluidic single cell analysis and received his Ph.D. in 2013. Currently he is investigating fiber probes for medical issues at the Institute of Physical Chemistry of Friedrich Schiller University Jena.

Dinglong Ma is a graduate student in the Department of Biomedical Engineering in the University of California, Davis. He has been working on real-time multi-spectral time-resolved fluorescence spectroscopy (ms-TRFS) for surgical guidance and automated intravascular ultrasound (IVUS) and fluorescence lifetime imaging (FLIm) bimodal technique for intravascular imaging.

Ines Latka studied physics at the Technical University Ilmenau and Friedrich Schiller University Jena. After her diploma thesis she worked for several years in the field of fiber optic sensors mainly for structural health monitoring, particularly with fiber Bragg gratings. In 2009 she joined the molecular imaging group at the Institute of Photonic Technology in Jena, Germany. Since 2013 she has been with the Institute of Physical Chemistry at Friedrich Schiller University Jena. Her current inter ests are focused on the development of in vivo qualified fiber optic probes based on linear and nonlinear Raman modalities.

Thomas Bocklitz studied physics and mathematics at Friedrich Schiller University. He received his diploma in theoretical physics in 2007 and a Ph.D. in chemometrics in 2011. He is a junior research group leader for statistical data analysis and image analysis mostly for biophotonic applications. His research agenda is closely connected with the translation of physical information, measured by AFM, TERS, Raman spectroscopy, CARS, SHG, and

TPEF, into medical or biologically relevant information. This research led to 30 publications in peer-reviewed journals, one patent, and one book chapter.

Brad Hartl is a Ph.D. candidate in the Department of Biomedical Engineering at the University of California, Davis. His work primarily focuses on utilizing Cerenkov luminescence as a light source to activate the photodynamic therapy process and also using fluorescence lifetime imaging to delineate radiation-induced necrosis from recurrent brain tumors and healthy tissues.

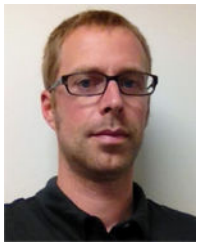

Julien Bec is a research engineer in the UC Davis Biomedical Engineering Department, working on nuclear imaging as well as optical imaging instrumentation. He is currently developing fiber-based probes and devices for fluorescence lifetime imaging with a particular focus on the development of multimodal imaging systems combining optics and ultrasound for intravascular applications.

Hussain Fatakdawala received his B.S. in Biomedical Engineering in 2009 from Rutgers University, New Brunswick, NJ, USA. He is currently pursuing his Ph.D. in biomedical engineering at the University of California Davis, Davis, CA, USA. His doctoral research work includes the application of fluorescence lifetime imaging and ultrasound for assessment and characterization of atherosclerotic plaques, cancer, and engineered tissues.

Eric Marple has been manufacturing fiber optic probes for the past 20 years, and has been a founder/principle of EmVision LLC since 2006. After graduating from The Pennsylvania State University with a B.S. in chemical engineering (1987), he has focused on the design and manufacture of small dimensioned fiber optic probes utilizing Raman spectroscopy for medical and industrial applications. He has numerous patents, and his patented probe technology allows for multiple spectroscopic techniques to be used in the same fiber-based probe, gathering all spectra from the same sample spot. He is currently working on fiber optic probes for in vivo applications.

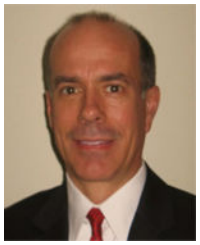

Kirk Urmey is a principle for EmVision LLC., a company specializing is fiber optic probes for use in medical and industrial applications. After graduating from The Ohio State University with a B.S. in electrical engineering (1986), Kirk has spent the last 25 years working in a variety of high technology fields. Kirk is the co-inventor on several patents directed at miniature probe designs that are targeting in vivo diagnostic applications. He is currently working on developing specialized manufacturing equipment for the production of the miniature fiber optical probe.

Sebastian Wachsmann-Hogiu is a professor in the Department of Pathology and Laboratory Medicine at the University of California, Davis, and is also affiliated with the Center for Biophotonics at the same institution. He received his Ph.D. in experimental physics from Humboldt University in Germany and his interests are in the fields of advanced optical techniques and nanobiophotonics with applications to biology and medicine.

Michael Schmitt received his Ph.D. in chemistry from the University of Würzburg in 1998. From 1999 to 2000 he conducted postgraduate studies at the Steacie Institute for Molecular Sciences at the National Research Council of Canada. He subsequently joined the group of Prof. Kiefer at the University of Würzburg, where he finished his habilitation in 2004. Since March 2004 he has been a research associate in the group of Prof. Jürgen Popp at the Institute for Physical Chemistry at Frie drich-Schiller-Universität Jena. His main research interests are focused on non-linear spectroscopy.

Laura Marcu is a professor of biomedical engineering and neurological surgery, and the head of the Biophotonics Laboratory at the University of California, Davis. Her research interests include the development of fluorescence-based instrumentation and methodologies which enable studies of the molecular, metabolic, and morphologic changes in living systems ranging from biological cells and animal models of human diseases to human patients. Her applied research has targeted solutions for main societal problems including atherosclerotic cardiovascular disease and cancer. She is an elected Fellow of OSA, SPIE, AIMBE, and BMES.

Jürgen Popp studied chemistry at the universities of Erlangen and Würzburg. After his Ph.D. in chemistry he joined Yale University for postdoctoral work. He subsequently returned to Würzburg University where he finished his habilitation in 2002. Since 2002 he has held a chair for physical chemistry at Friedrich Schiller University Jena. Since 2006 he has also been the scientific director of the Leibniz Institute of Photonic Technology, Jena. His research interests are mainly concerned with biophotonics. In particular his expertise in

the development and application of innovative Raman techniques for biomedical diagnosis should be emphasized.

References

1. Coda S, Thillainayagam AV. State of the art in advanced endoscopic imaging for the detection and evaluation of dysplasia and early cancer of the gastrointestinal tract. Clin Exp Gastroenterol. 2014; 7:133–150. [PubMed: 24868168]
2. Flusberg BA, Cocker ED, Piyawattanametha W, Jung JC, Cheung ELM, Schnitzer MJ. Fiber-optic fluorescence imaging. Nat Methods. 2005; 2:941–950. [PubMed: 16299479]
3. Movasaghi Z, Rehman S, Ihtesham D, Rehman U. Raman spectroscopy of biological tissues. Appl Spectrosc Rev. 2007; 42:493–541.
4. Tu Q, Chang C. Diagnostic applications of Raman spectroscopy. Nanomedicine. 2012; 8:545–558. [PubMed: 22024196]
5. Eberhardt K, Stiebing C, Matthäus C, Schmitt M, Popp J. Advantages and limitations of Raman spectroscopy for molecular diagnostics: an update. Expert Rev Mol Diagn. 2015 doi: 10.1586/14737159.2015.1036744.
6. Krafft C, Dochow S, Latka I, Dietzek B, Popp J. Diagnosis and screening of cancer tissues by fiber-optic probe Raman spectroscopy. Biomed Spectrosc Imaging. 2012; 1:39–55. doi:10.3233/BSI-2012-0004.
7. Latka I, Dochow S, Krafft C, Dietzek B, Popp J. Fiber optic probes for linear and nonlinear Raman applications—current trends and future development. Laser Photonics Rev. 2013; 7:698–731. doi: 10. 1002/lpor.201200049.
8. Wang W, Zhao J, Short M, Zeng H. Real-time in vivo cancer diagnosis using Raman spectroscopy. J Biophotonics. 2014; 19:1–19. doi: 10.1002/jbio.201400026.
9. Patil CA, Kirshnamoorthi H, Ellis DL, van Leeuwen TG, Mahadevan-Jansen A. A clinical instrument for combined Raman spectroscopy-optical coherence tomography of skin cancers. Lasers Surg Med. 2011; 43:143–151. [PubMed: 21384396]
10. Kong K, Rowlands CJ, Varma S, Perkins W, Leach IH, Koloydenko AA, Williams HC, Notingher I. Diagnosis of tumors during tissue-conserving surgery with integrated autofluorescence and Raman scattering microscopy. PNAS. 2013; 110:15189–15194. [PubMed: 24003124]
11. Šćepanović OR, Fitzmaurice M, Gardecki JA, Angheloiu GO, Awasthi S, Motz JT, Kramer JR, Dasari RR, Feld MS. Detection of morphological markers of vulnerable atherosclerotic plaque using multimodal spectroscopy. J Biomed Opt. 2006; 11:021007. doi:10.1117/1.2187943. [PubMed: 16674182]
12. Sharma M, Marple E, Reichenberg J, Tunnell JW. Design and characterization of a novel multimodal fiber-optic probe and spectroscopy system for skin cancer applications. Rev Sci Instrum. 2014; 85:083101. doi:10.1063/1.4890199. [PubMed: 25173240]
13. Šćepanović OR, Fitzmaurice M, Miller A, Kong C-R, Volynskaya Z, Dasari RR, Kramer JR, Feld MS. Multimodal spectroscopy detects features of vulnerable atherosclerotic plaque. J Biomed Opt. 2011; 16:011009–1–011009-10. [PubMed: 21280896]
14. Sun Y, Phipps JE, Meier J, Hatami N, Poirier B, Elson DS, et al. Endoscopic fluorescence lifetime imaging for in vivo intraoperative diagnosis of oral carcinoma. Microsc Microanal. 2013; 19:791–798. [PubMed: 23702007]
15. Cheng S, Rico-Jimenez JJ, Jabbour J, Malik B, Maitland KC, Wright J, et al. Flexible endoscope for continuous in vivo multispectral fluorescence lifetime imaging. Opt Lett. 2015; 38:1515–1517. [PubMed: 23632536]
16. Sparks H, Warren S, Guedes J, Yoshida N, Charn TC, Guerra N, et al. A flexible wide-field FLIM endoscope utilising blue excitation light for label-free contrast of tissue. J Biophotonics. 2014; 11:1–11. doi:10.1002/jbio.201300203.
17. Ma D, Bec J, Yankelevich D, Gorpas D, Fatakdawala H, Marcu L. Rotational multispectral fluorescence lifetime imaging and intravascular ultrasound: bimodal system for intravascular applications. J Biomed Opt. 2014; 19(6):066004. [PubMed: 24898604]

18. Yankelevich DR, Ma D, Liu J, Sun Y, Sun Y, Bec J, Elson DS, Marcu L. Design and evaluation of a device for fast multi-spectral time-resolved fluorescence spectroscopy and imaging. Rev Sci Instrum. 2014; 85:034303. [PubMed: 24689603]

19. Liu J, Sun Y, Qi JY, Marcu L. A novel method for fast and robust estimation of fluorescence decay dynamics using constrained least-squares deconvolution with Laguerre expansion. Phys Med Biol. 2012; 57:843–865. [PubMed: 22290334]

20. Butte PV, Pikul BK, Hever A, Yong WH, Black KL, Marcu L. Diagnosis of meningioma by time resolved fluorescence spectroscopy. J Biomed Opt. 2005; 10(6):064026–1–064026-9. [PubMed: 16409091]

21. Sun YH, Hatami N, Yee M, Elson DS, Gorin F, Schrot RJ, Marcu L. Fluorescence lifetime imaging microscopy for brain tumor image-guided surgery. J Biomed Opt. 2010; 15(5):056022. [PubMed: 21054116]

22. Butte PV, Mamelak AN, Nuno M, Bannykh SI, Black KL, Marcu L. Fluorescence lifetime spectroscopy for guided therapy of brain tumors. NeuroImage. 2012; 54:125–135.

23. McCreery, RL. Raman spectroscopy for chemical analysis. Vol. 225. Wiley; New York: 2005.

24. Mandair GS, Morris MD. Contributions of Raman spectroscopy to the understanding of bone strength. BoneKEy Rep. 2015; 4:620. doi:10.1038/bonekey.2014.115. [PubMed: 25628882]

25. Bergner N, Bocklitz T, Romeike BFM, Reichartd R, Kalff R, Krafft C, Popp J. Identification of primary tumors of brain metastases by Raman imaging and support vector machines. Chemometr Intell Lab Syst. 2012; 117:224–232.

26. Wood BR, Caspers P, Puppels GJ, Pandiancherri S, McNaughton D. Resonance Raman spectroscopy of red blood cells using near-infrared laser excitation. Anal Bioanal Chem. 2007; 387:1691–16703. [PubMed: 17151857]

27. Huang Z, Zeng H, Hamzavi I, McLean DI, Lui H. Rapid near-infrared Raman spectroscopy system for real-time in vivo skin measurements. Opt Lett. 2001; 26:1782–1784. [PubMed: 18059697]

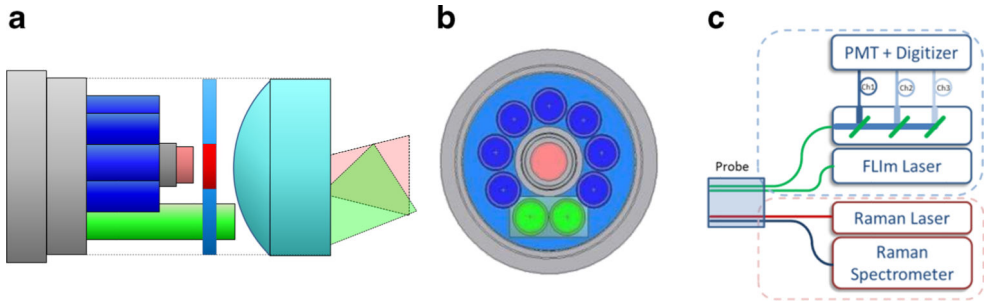

Fig. 1.

a Schematic view of the probe with filters, lenses, and beam propagation cones. **b** Front view of the probe distal end. The fibers shown in *blue* are used for collecting the Raman scattering. The fiber shown in *red* is a 300-μm-core fiber that transmits the light for the Raman excitation. The fibers shown in *green* are 300-μm-core fibers for generating the FLIm signal. **c** Overview of the complete setup which was used for the bimodal FLIm and Raman acquisition

b

Raman fuzzy clustering

Fit #	Estimated res. (pixel)
1	3.25
2	6.91
3	7.97
4	6.65
5	5.50
6	5.94
7	4.77
8	5.03
9	2.65
10	7.18
Average	5.59
Distance / pixel	42.50
Resulting res.	237.36

FLIm intensity map

Intensity profile #	Interpolated res. (pixel)
1	5.61
2	6.16
3	5.86
4	7.53
5	7.03
6	6.80
7	4.78
8	6.15
9	6.33
10	5.31
Average	6.16
Distance / pixel	42.50
Resulting res.	261.63

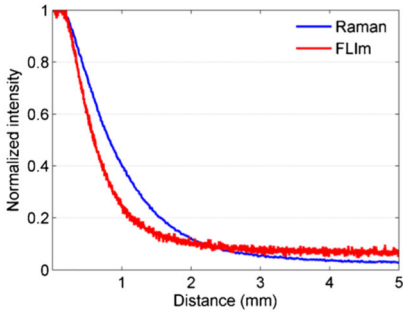

Fig. 2.

a Determination of the lateral resolution for FLIm and Raman with indicated measurement lines in the images and corresponding estimated resolutions (**b**). **c** Intensity of the Raman/ fluorescence signal during a pullback sequence

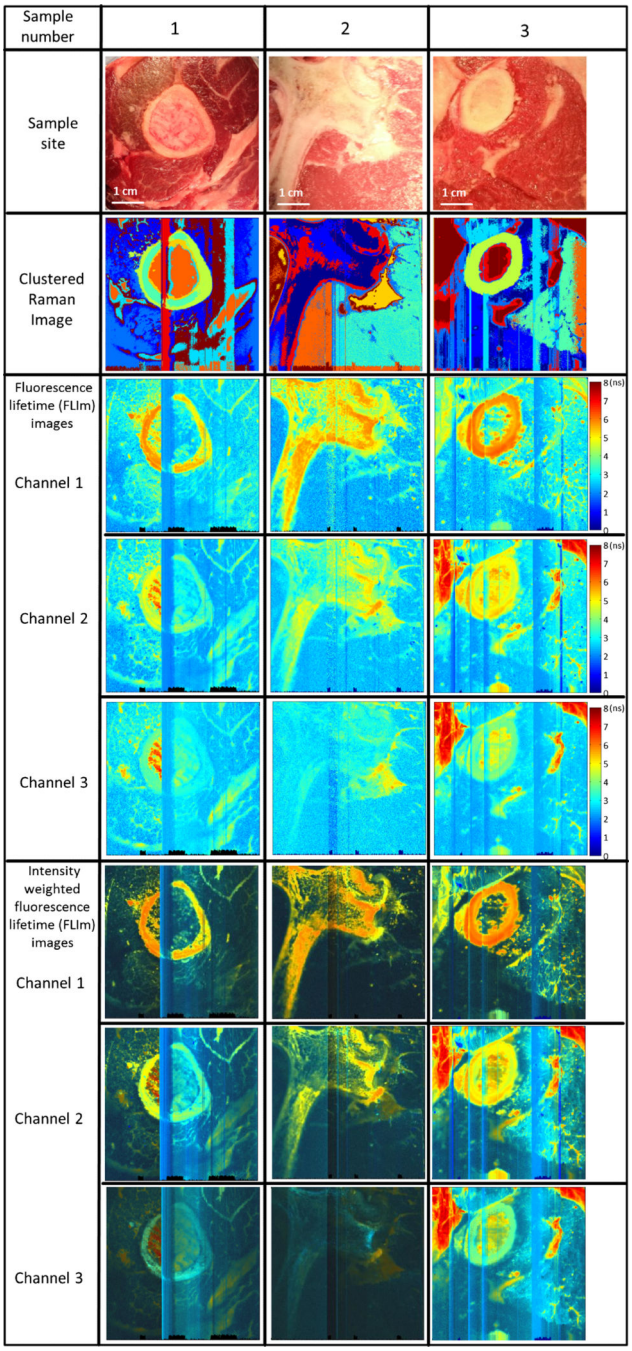

Fig. 3.

Image comparison between FLIm and Raman spectroscopy: *Sample 1* lamb, *2* beef, *3* lamb. The *stripes* are residual probe tip artifacts if the probe is in close contact with the sample. The area of all images is 50×50 mm and corresponds to 400×400 spectra for both modalities

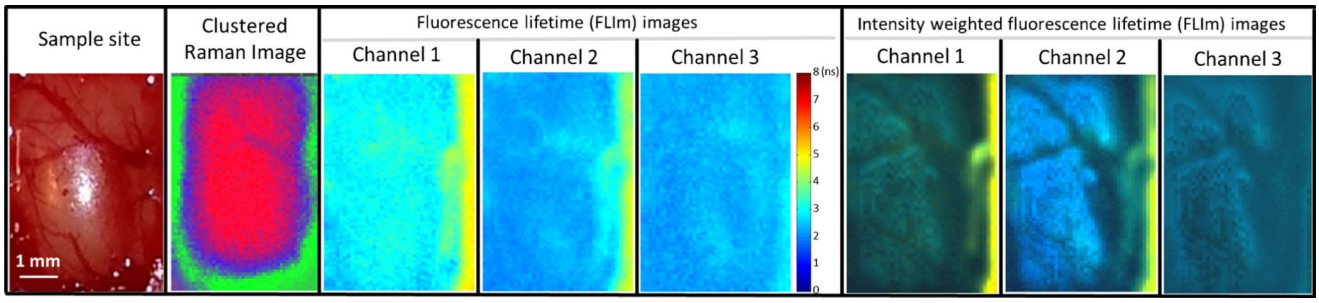

Fig. 4.

In vivo bimodal mapping of a rat's dura. The cortex shows a rather uniform lifetime contribution and the blood vessels of the dura are only visible in Raman and the intensity-weighted lifetime maps

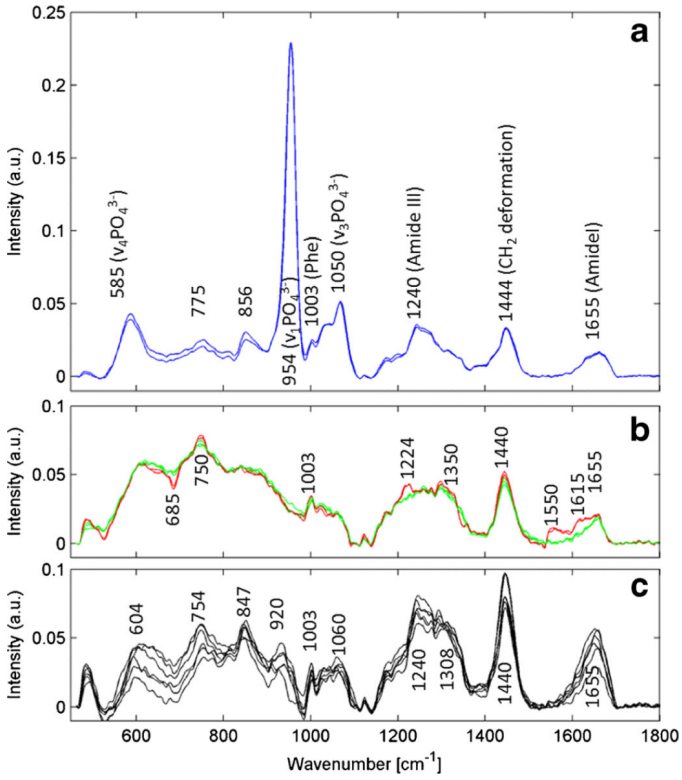

Fig. 5.

In vivo acquired Raman spectra of **a** bone, **b** brain (*green*) and blood vessels overlaid with a spectrum of brain tissue (*red*) in comparison with a Raman spectrum of **c** skin